WIND ENERGY
Wind Energ. 0000; **00**:1–15
DOI: 10.1002/we

RESEARCH ARTICLE

An experimental investigation on the effect of individual turbine control on wind farm dynamics

Jennifer Annoni[1], Kevin Howard[2], Peter Seiler[1], and Michele Guala[2]

[1]Aerospace Engineering and Mechanics, University of Minnesota
[2]Civil, Environmental and Geo-Engineering and Saint Anthony Falls Laboratory (SAFL), University of Minnesota

ABSTRACT

Individual wind turbines in a wind farm typically operate to maximize their performance with no consideration of the impact of wake effects on downstream turbines. There is potential to increase power and reduce structural loads within a wind farm by properly coordinating the turbines. To effectively design and analyze coordinated wind turbine controllers requires control-oriented turbine wake models of sufficient accuracy. This paper focuses on constructing such a model from experiments. The experiments were conducted to better understand the wake interaction and impact on voltage production in a three-turbine array. The upstream turbine operating condition was modulated in time and the dynamic impact on the downstream turbine was recorded through the voltage output time signal. The flow dynamics observed in the experiments were used to improve a static wake model often used in the literature for wind farm control. These experiments were done in the atmospheric boundary layer wind tunnel at the Saint Anthony Falls Laboratory (SAFL) at the University of Minnesota using particle image velocimetry (PIV) for flow field analysis and turbine voltage modulation to capture the physical evolution in addition to the dynamics of turbine wake interactions.

KEYWORDS

wind farm control; wake interactions; system identification

Correspondence

University of Minnesota 110 Union St SE, Minneapolis, MN 55455 . E-mail: anno0010@umn.edu

Contract/grant sponsor

This work was supported by the National Science Foundation under Grant No. NSF-CMMI-1254129 entitled “CAREER: Probabilistic Tools for High Reliability Monitoring and Control of Wind Farms.” Any opinions, findings, and conclusions or recommendations expressed in this material are those of the authors and do not necessarily reflect the views of the NSF. Additional funding was provided through the Initiative for Renewable Energy and the Environment at the University of Minnesota.

Received . . .

1. INTRODUCTION

Many state governments in the U.S. have renewable portfolio standards that mandate renewable energy targets. For example, Minnesota has a target of 25% renewable energy by 2025 [1]. Wind energy is a fast growing source of renewable energy, hence it represents a key area to improve. Achieving these targets requires an increase in the efficiency of existing wind farms by maximizing power production and minimizing structural loads on the turbines. Reducing structural loads on turbines will improve the economic competitiveness of wind energy by reducing the operation and maintenance costs and increasing the lifetime of turbines, thus promoting new capital investments.

Currently, wind turbines are typically controlled individually to maximize their own performance. Studies have shown that operating all turbines within a wind farm at their optimal operating point, leads to suboptimal performance of the overall wind farm [2, 3, 4, 5]. An improved understanding of the aerodynamic interactions between turbines can aid in the design of enhanced control strategies that coordinate all turbines in a farm. There have been some studies in the field and in wind tunnels looking at these aerodynamic interactions [6, 7, 8]. The coordinated turbine control strategies presented in the literature aim to increase the total wind farm power and, in some cases, reduce the structural loads. The essential idea is that reducing the efficiency of the lead turbines, referred to hereafter as derating, results in higher wind speeds for downstream turbines. Proper derating can result in a higher total wind farm production as compared with simply operating each turbine

Prepared using weauth.cls [Version: 2010/06/17 v1.00]

at its own peak efficiency. Industry leaders, such as General Electric, have investigated and successfully implemented some wind farm control strategies [9].

Most of the prior work on coordinated turbine control has used simplified actuator disk models for the design and analysis. More accurate wake modeling is necessary to help understand and quantify the aerodynamic interactions in a wind farm. A variety of wake models exist in the literature that are useful for studying wind farm control. The simplest, quasi-static models are the Park model [10] and the eddy viscosity model [11]. These models provide a fast, preliminary description of the wake interactions in a wind farm, but neglect some key dynamics, such as effects due to large-scale turbulent structures and wake meandering [12]. Some additional studies have been done to extend the Park model to include additional dynamics [13, 14, 15, 16].

This paper focuses on experiments conducted in a wind tunnel that help highlight limitations of the static Park model, typically used in wind farm control literature, and presents a dynamic Park model derived from experimental data. Section 2 describes the Park model and some of the wake characteristics essential for wind farm control in detail. The Park model is compared to experiments that were done in the atmospheric boundary layer wind tunnel at SAFL using a three turbine setup with model turbines, aligned in the wind direction, described in Section 3. The results from the comparison are presented in Section 4 along with some suggestions on how to improve the Park model to account for the flow dynamics. Section 4 also describes how the experimental data is used to construct a dynamic model that can be used for control of a three turbine array. Lastly, Section 5 discusses the future work using wind farm control in the wind tunnel.

2. TURBINE WAKE MODELING

2.1. Wake Characteristics

Individual turbine control has a significant impact on the flow dynamics in the wake. The wind turbine operation creates a trailing wake that is commonly divided into two regions [17]: the near wake and the far wake (see Figure 1). The near wake is roughly defined as the region directly downstream of the turbine where characteristics of the flow field are determined by the turbine geometry, i.e. the rotor and hub height, the blades, and the nacelle. The flow is driven by a strong non-zero pressure gradient and significant turbulence associated with the tip and trailing vortices enhanced by the shear layer produced by the separation of the flow at the blade edges. In the far wake, the pressure gradient becomes less significant. The wake is less dependent on the turbine geometry and more on topographic and thermal stability effects, in addition to any large-scale in-homogeneity of the incoming flow. In flat terrain, this region is approximately axisymmetric and self-similar making it easier to model [18]. The transition between the near and the far wake may be dependent on turbine controls. For more details, see [19].

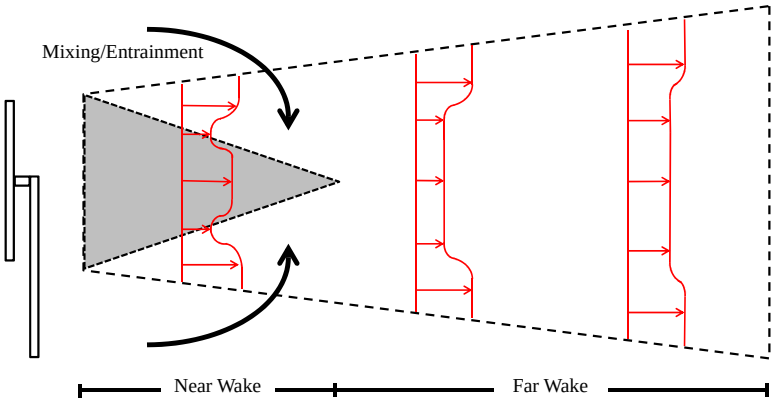

Figure 1. Distinction between different regions in the wake

One important flow characteristic in the far wake is the turbulence intensity. The turbulence generated in the wake can have a significant impact on wind farm control as it dictates much of the evolution of the wake as it propagates downstream. The turbulence in the wake is driven by the interaction between the ambient turbulence advected by the mean wind and the turbulence generated by the turbine. As the wind passes through the leading turbines, the flow separates from the blades and around the tower/nacelle and generates a complex 3D flow structure with higher turbulent kinetic energy. The flow field also experiences a velocity deficit due to the power extraction from the turbine. This velocity deficit defines the wake, and a shear layer separates the wake from the freestream velocity. This shear layer contains vortices that entrain high

Wind Energ. 0000; **00**:1–15 © 0000 John Wiley & Sons, Ltd.
DOI: 10.1002/we
Prepared using weauth.cls

momentum fluid, i.e. transports fluid momentum from outside the wake to inside the wake, causing the wake to expand and recover downstream of the turbine. On average the turbulence intensity increases as it passes through the next turbine downstream and the rate of entrainment increases the amount of turbulence and results in a faster recovery rate [20].

Another important wake characteristic is wake meandering. This is characterized as cyclical motions of the wake, particularly notable in the vertical and spanwise directions, which is caused by the interactions of large-scale turbulent structures in the wake [21, 22]. Wake meandering can have a significant impact on the structural loads of downstream turbines. However, wake meandering can help recover the power loss that is expected of turbines downstream in a wind farm by increasing mixing as the wake deflects further into the freestream flow.

2.2. Static Park Model

The static wake model typically used in the literature for wind farm control is the Park Model [10]. The Park Model has a low computational cost due to its simplicity. It is based on the assumptions that there is a steady inflow, linear wake expansion, and the velocity in the wake is uniform at a cross section downstream. The turbine is modeled as an actuator disk with uniform axial loading.

Consider the example of a turbine operating in a freestream velocity U_∞. The diameter of the turbine rotor is denoted by D and the turbine is assumed to be operating at an axial induction factor a. The induction factor is a measure of how much the wind slows down due to the action of the turbine. In particular, the induction factor for a single turbine is defined as $a := 1 - \frac{u}{U_\infty}$, where u denotes the average horizontal flow velocity across the rotor plane and U_∞ denotes the freestream velocity. In practice, the induction factor can be related to the blade pitch angle and the generator torque, which are standard inputs to a utility-scale turbine [23, 24]. A cylindrical coordinate system is placed at the rotor hub of the first turbine with the downstream and radial distances denoted by x and r. The velocity profile at a location (x, r) is:

$$u(x, r; a) = U_\infty(1 - \delta u(x, r; a)) \tag{1}$$

where the velocity deficit δu is given by

$$\delta u = \begin{cases} 2a\left(\frac{D}{D+2kx}\right)^2, & \text{if } r \leq \frac{D+2kx}{2}, \\ 0, & else \end{cases} \tag{2}$$

In this model, u is defined as the velocity in the downstream/axial (x) direction, and the remaining velocity components are neglected. The wake is parameterized by a tuneable nondimensional wake expansion coefficient, k [25]. The wake expansion coefficient provides an averaged notion of turbulence in the Park model. This model is developed based on idealistic conditions and does not address the flow dynamics in a wind farm. Also, this model (1), (2) is a description of a single turbine wake. Extensions to include more turbines can be seen in [26],[27].

As mentioned previously, the turbine is modeled as a porous actuator disk having constant, radial, or variable loading that influences the flow field. The advantage to using the actuator disk is that the blades of the turbine do not have to be modeled, which reduces the overall computation time. When using an actuator disk to represent a turbine, the axial induction factor, a, provides an input to describe the turbine operation. The induction factor can be related to the power and thrust coefficient of a turbine. The axial thrust force (perpendicular to the rotor plane) is given by $T = \frac{1}{2}\rho A u^2 C_T$ where C_T is the thrust coefficient. The power of the turbine is defined as $P = \frac{1}{2}\rho A u^3 C_P$ where C_P is the power coefficient. Specifically, C_T and C_P can be written as a function of the axial induction factor, a [23]:

$$C_T(a) = 4a(1 - a) \tag{3}$$

$$C_p(a) := 4a(1 - a)^2 \tag{4}$$

The maximum of the power coefficient (4) is $C_{P,max} = 0.593$ achieved at an induction factor of $a = \frac{1}{3}$, see Figure 2. This is the Betz limit for turbine efficiency [23]. These are idealized relationships between C_T, C_P and a for the actuator disk. Typical utility-scale turbines have a $C_P = 0.4 - 0.5$. Operating turbines at their maximum operating point may not be the optimal operating point of the whole wind farm. There is the potential to increase overall production out of a wind farm by operating the front turbines suboptimally [4].

Suboptimal performance of the front turbines is achieved by decreasing the power captured by the front turbine(s). This allows the downstream turbine(s) to capture more power. Increasing or decreasing the induction factor from the optimal has different effects on the flow dynamics in the wake. For example, a decrease in the induction factor is equivalent to moving left of the peak on the C_P curve in Figure 2, and corresponds to a decrease in C_T. Decreasing the thrust generated by the turbine leads to less turbulent kinetic energy in the wake directly behind the upstream turbine. Alternatively, increasing the induction factor from the optimal, results in an increase in the thrust coefficient. This will increase the level of turbulence in the wake of the upstream turbine, which will induce more mixing, and the velocity in the wake will recover to freestream

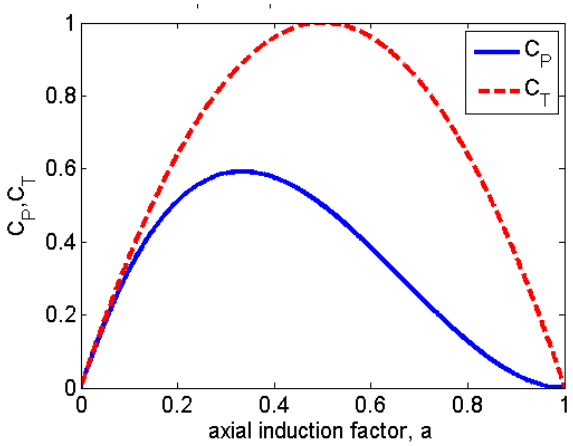

Figure 2. Cp vs. Ct of an ideal turbine

at a faster rate. The downstream turbine may see a higher incoming velocity resulting in more available power, due to an increase in thrust. This increase in velocity is dependent on the local conditions, such as ambient turbulence and atmospheric stability. It is important to note that it is also possible, depending on the local conditions, that there is a decrease in velocity at the downstream turbine due to the increase in thrust at the upstream turbine [28]. Increasing the thrust of the upstream turbine can increase structural loading at the downstream turbine and can increase the effects of wake meandering due to the increase in turbulence. The effects of the flow dynamics caused by the interaction of flow turbulence and wake meandering are not specifically addressed or modeled in these simplified models.

2.3. Dynamic Park Model

The static Park model (Section 2.2) can be generalized to include turbine dynamics and the effects of wake transport. This section describes a dynamic formulation of the Park model, hereafter referred to as the dynamic Park model. The dynamic Park model includes models for the upstream and downstream turbine dynamics as well as the wake transport. A block diagram of this dynamic Park model is shown in Figure 3. The following subsections describe the models used for the turbine dynamics and wake transport. Then a complete linearized model is derived for the dynamic Park model. This linearized dynamic model can be used for wind farm control in the wind tunnel.

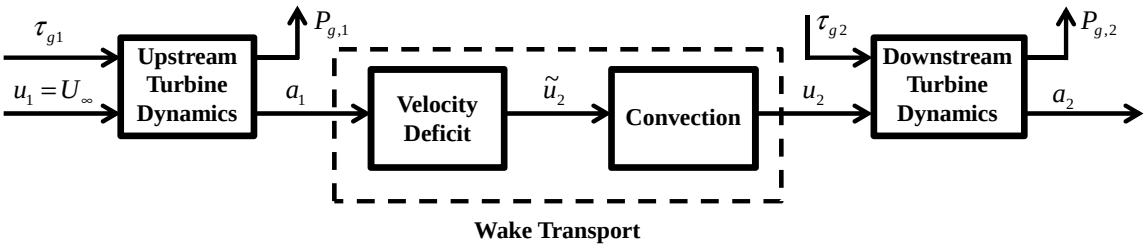

Figure 3. Block Diagram of the Dynamic Park model

2.3.1. Turbine Dynamics

Section 2.2 discussed a static turbine model with the axial induction factor, a, as the controllable input. For this static model, the power coefficient, $C_P(a)$, has a cubic dependence on induction (4). An actual utility-scale turbine has blade pitch, β [rad], and generator torque, τ_g [Nm], as controllable inputs. In our experiments the blade pitch, β, is held fixed. Hence the model described in this section includes only generator torque as the controllable input. Constant blade pitch corresponds, for a utility-scale turbine, to operation in low wind speed (Region 2) conditions. If β is constant then the aerodynamic forces on the turbine depend only on the nondimensional tip-speed ratio (TSR) defined as $\lambda := \frac{\omega R}{u}$ where ω [rad/s] is the rotor speed. For this more realistic model, the power coefficient is given by a function $C_P(\lambda)$. The captured power and aerodynamic torque can then be expressed as $P_c = \frac{1}{2}\rho A u^3 C_P(\lambda)$ [W] and $\tau_{aero} := \frac{P_c}{\omega}$ [Nm]. This leads to the following simplified, single degree-of-freedom rotor dynamic for the turbine:

DOI: 10.1002/we
Prepared using weauth.cls

$$\dot{\omega} = \frac{1}{J}\left(\tau_{aero} - \tau_g\right) \tag{5}$$

where $\dot{\omega}$ [rad/sec^2] is the angular acceleration of the rotor shaft and J [kgm^2] is the rotational inertia. Equation 5 is simply Newton's second law for the rotational dynamics of the rotor shaft. Many details of the actual turbine dynamics, e.g. tower/blade flexibility, have been neglected in this one-state model. However, it is sufficient to capture the key dynamics at the wind farm scale.

The outputs for this simplified turbine model will be the generated power P_g and the induction factor a. The generated power is given by $P_g = \tau_g \omega$ [W] and this represents the power converted to useful electrical power. The generated and captured powers are the same in steady state. However, they can differ in transient scenarios as some energy goes to acceleration/decceleration of the rotor shaft. The axial induction factor a of a turbine is the result of the operating conditions of the turbine. Specifically, a depends only on the tip-speed ratio, i.e. $a(\lambda)$. Blade element momentum theory can be used to derive expressions for $C_P(\lambda)$ and $a(\lambda)$ in terms of the geometric and aerodynamic properties of the turbine blades [23]. The lift to drag ratio of the turbine blades is a key parameter in these models.

The simplified nonlinear turbine dynamics consist of the rotor dynamics (5) along with the expressions for a, C_P, λ, and τ_{aero}. Specifically, the model has one state (ω), one controllable input (τ_g), one disturbance input (u), and two outputs (P_g and a). The state derivative and outputs can be completely expressed in terms of the state and inputs as follows:

$$\dot{\omega} = \frac{1}{J}\left(\frac{\rho A u^3 C_P\left(\frac{\omega R}{u}\right)}{2\omega} - \tau_g\right) := f(\omega, \tau_g, u) \tag{6}$$

$$\begin{bmatrix} P_g \\ a \end{bmatrix} = \begin{bmatrix} \tau_g \omega \\ a\left(\frac{\omega R}{u}\right) \end{bmatrix} := h(\omega, \tau_g, u) \tag{7}$$

This same dynamic model is used for both the upstream and downstream turbines. For the upstream turbine, the wind speed across the rotor plane is given by the freestream velocity, i.e. $u = U_\infty$. For the downstream turbine, the wind speed across the rotor plane, $u = u_2$, depends on the (time-dependent) velocity in the wake.

2.3.2. Wake Transport

The turbine dynamics described in the previous section are used to compute the time-varying axial induction for the upstream turbine, $a_1(t)$. In steady-state situations, the (static) Park model (2) can be used to compute the downstream velocity deficit due to the axial induction of the upstream turbine. In time-varying situations, the actions of the upstream turbine are not instantaneously observed at the downstream turbine. The time it takes for the wake to propagate downstream depends on the convection velocity and the distance between the turbines.

The wake transport model used here consists of the (static) Park model to determine the velocity deficit and a time delay τ_d to account for convection delay. Assume the downstream turbine is fully operating in the wake of the upstream turbine and is located a distance x behind the upstream turbine. The time-varying velocity at the rotor plane of the downstream turbine is given by:

$$\tilde{u}_2(t) = u_1(t)\left(1 - 2a_1(t)\left(\frac{D}{D + 2kx}\right)^2\right) \tag{8}$$

$$u_2(t) = \tilde{u}_2(t - \tau_d) \tag{9}$$

These equations define the wake transport. Specifically, (8) accounts for the velocity deficit while (9) accounts for the convection delay. In other words, the velocity at the downstream turbine at time t depends on the actions of the upstream turbine at time $t - \tau_d$. The convection delay should depend on the velocity in the wake. For simplicity, we approximate this convection delay using the free-stream velocity, $\tau_d = \frac{x}{U_\infty}$.

2.3.3. Linearized Model

A nonlinear model for many turbines operating in a line can be constructed by linking together the models described previously for the turbine dynamics and wake transport. This formulation provides insight into the aerodynamic coupling that occurs within a wind farm. Section 4.2 compares the dynamic Park model with data obtained from wind tunnel experiments. Specifically, a linearized model for the wind farm is used as a the basis for comparison. This subsection briefly describes the construction of the linearized dynamics for two turbines. The derivation can easily be extended to three or more turbines.

The linearization is constructed about an equilibrium trim condition. Specifically, assume the generator torque and wind speed inputs to the upstream turbine are held constant at $\overline{\tau}_{g,1}$ and $\overline{u}_1 = U_\infty$, respectively. The upstream turbine will reach

an equilibrium rotor speed $\overline{\omega}_1$, generated power $\overline{P}_{g,1}$, and axial induction $\overline{a}_1$. The (static) Park model gives the downstream velocity in steady conditions as $\overline{u}_2 = \overline{u}_1 \left(1 - \overline{a}_1 \left(\frac{D}{D+2kx}\right)^2\right)$. Finally, if the generator torque at the downstream turbine is held constant at $\overline{\tau}_{g,2}$, then the downstream rotor will reach an equilibrium state/output of $(\overline{\omega}_2, \overline{P}_{g,2}, \overline{a}_2)$. This collection of constant values (denoted by overbars) defines an equilibrium trim condition for the two-turbine array.

Deviations from the trim conditions are denoted using δ, e.g. $\delta\tau_g(t) = \tau_g(t) - \overline{\tau}_g$. The nonlinear turbine dynamics has only one state. Hence the linearized dynamics for the upstream and downstream turbines have the following transfer function form:

$$\begin{bmatrix} \delta P_{g,i}(s) \\ \delta a_i(s) \end{bmatrix} = \frac{N_i}{s + p_i} \begin{bmatrix} \delta\tau_{g,i}(s) \\ \delta u_i(s) \end{bmatrix} \quad \text{where} \quad i = 1, 2 \tag{10}$$

where p_i are scalars and N_i are 2 x 2 matrices for $i = 1, 2$. The wake transport consists of a nonlinear function and a pure time delay. Hence the linearized wake transport contains no dynamics and can be represented in the frequency domain by:

$$\delta u_2(s) = e^{-s\tau_d} D_{Park} \begin{bmatrix} \delta a_1(s) \\ \delta u_1 \end{bmatrix} \tag{11}$$

where D_{Park} is a 1 x 2 matric gain. The linearized components can be combined to obtain a linear model for the two turbine array. For example, the wind tunnel experiments roughly corresponds to varying the upstream generator torque and measuring the downstream power. The transfer function from $\delta\tau_{g,1}$ to δP_2 is then given by:

$$G_{\delta\tau_{g,1}\to\delta P_2}(s) = G_{\delta\tau_{g,1}\to\delta a_1}(s) G_{\delta a_1\to\delta u_2}(s) G_{\delta u_2\to\delta P_2}(s) \tag{12}$$

$$= \frac{(N_2)_{12}}{s + p_2} \cdot e^{(-s\tau_d)} (D_{Park})_{11} \cdot \frac{(N_2)_{21}}{s + p_1} \tag{13}$$

Note that this linearized model corresponds to a second order system with a pure time delay. The experimental results provided in Section 4.2 can be accurately fit with a model of this form.

3. EXPERIMENTAL SETUP

3.1. Wind Tunnel

The experiments used to address wind farm modeling were completed in a closed loop wind tunnel at the Saint Anthony Falls Laboratory (SAFL) on the campus of the University of Minnesota. A 150 kW fan drives the flow into the tunnel test section, which has a length of 16 m and a cross-section of 1.7 m by 1.7 m. Coarse wire mesh and a honeycomb flow straightener condition the flow prior to entering a contraction with an area ratio of 6.6:1 upstream of the main test section. Immediately at the end of the contraction, a trip is placed to promote boundary layer growth. The model turbines were placed roughly 13 m downstream of the trip in the test section where a turbulent boundary layer thickness of $\delta \approx 0.6$ m was measured under thermally neutral conditions. The neutral cases investigated herein set the air and floor temperature equal, and were held to within $\pm 0.2^{\circ}$C. Mean and fluctuating flow statistics of the baseline turbulent boundary layer are provided in [29].

3.2. Turbine Model

The turbine models tested in the tunnel are approximately 1:750 scale models of the Clipper Liberty 2.5MW utility-scale wind turbine, see Figure 4. The resulting dimensions for the model are a three-blade rotor with a diameter of 0.128 m (GWS/EP-5030x3 rotor). While the original design for this rotor was for use on model aircraft, the blades herein were oriented such that the high pressure surface faced the inflow. In addition, the blade airfoil profiles are nearly flat. The hub height is 0.104 m and remains within the lower twenty-five percent of the boundary layer, similar to the full-scale turbine. The TSR, λ, was controlled by selecting the model turbine generator and is on the lower end of the λ range for turbines used in the field. This set of experiments uses a specific hub velocity of approximately 4.5 m/s. It is in the operating range of standard turbines and provides a detailed comparison to wind farm experiments completed at the same velocity. The free-spinning TSR for the model turbine in the undisturbed boundary layer is $\lambda \approx 4.5$, while typical values for utility-scale wind turbines range between $\lambda \approx 3.5$ and 10.

The model turbines have a small DC generator in which a voltage output can be measured or a voltage input can be applied to control the turbine operating condition. The DC voltage input is restricted to lie within +/-1.25V. A zero voltage input corresponds to a free spinning turbine. In this condition, the turbine operates at a high TSR. Applying a positive

DOI: 10.1002/we
Prepared using weauth.cls

Figure 4. Two turbine setup in the SAFL wind tunnel (left) and the 2.5 MW Clipper turbine at UMore Park (right)

voltage places a torque on the motor shaft causing the turbine to operate at a lower TSR. A properly chosen voltage results in the turbine operating near its optimal TSR, $\lambda = 3$. Thus the DC voltage input mimics the effect of the generator torque on a utility-scale turbine.

3.3. Three Turbine Setup

3.3.1. Operating Conditions

The model turbines were operated in two different states: (i) rated; (ii) derated, i.e. higher thrust In the rated state, a 1.25V input was applied from a DC power supply or function generator to the DC generator on the model turbine. This input applies a torque opposing the aerodynamic torque and controls the TSR. In the derated state, the turbine was allowed to operate under no load, i.e. a zero voltage input [30]. The rated case corresponds to a turbine operating near the peak of the C_P curve in Figure 2. The derated case corresponds to a turbine operating on the right side of the C_P curve which leads to a larger C_T and hence larger turbulence levels in the wake. In these experiments, the voltage generated by each turbine is similar to the power generated by a utility-scale turbine. For more details on turbine voltage production and analysis verification, the reader is directed to [30].

3.3.2. Experimental Conditions

These experiments consisted of three turbines placed in a row with a five diameter (5D) spacing between the turbines, see Figure 5. Each experiment was run at a wind speed of 4.5 m/s under a neutral boundary layer with 1.5% turbulence intensity for 100 s. This sample time was selected as it was the limit for the maximum number of samples for the data acquisition system when sampling at 10000 Hz. Wall parallel PIV was used to capture the varying physical characteristics in the wake created by the upstream and downstream turbines under rated and derated states with the overall goal of using the results to improve the Park model. This provides some insight as to how specific control actions of Turbine 1 affect the overall flow characteristics in the wake, and the use of wall parallel PIV simplified the problem by removing the extra factor of the boundary layer from the wake development. PIV uses a pulsating laser sheet synchronized with high resolution cameras to capture the instantaneous movement of seeding particles in the flow. Olive oil droplets on the order of 5 to 10 microns in diameter are injected into the wind tunnel and tracked by taking snapshots in time and comparing the locations of individual groups of particles to obtain the change in distance between the subsequent frames. The time between snapshots is known and, therefore, the velocity vectors of the particles can be computed using 2D spatial cross correlation in the interrogation windows in which the full image is subdivided (TSI PIV software). In this specific case, a fine 32x32 pixel^2 interrogation window is used with a 50% overlap, providing a spatial resolution of approximately 1.8mm in the streamwise and spanwise directions. Each run consisted of 700 snapshots over 100s.

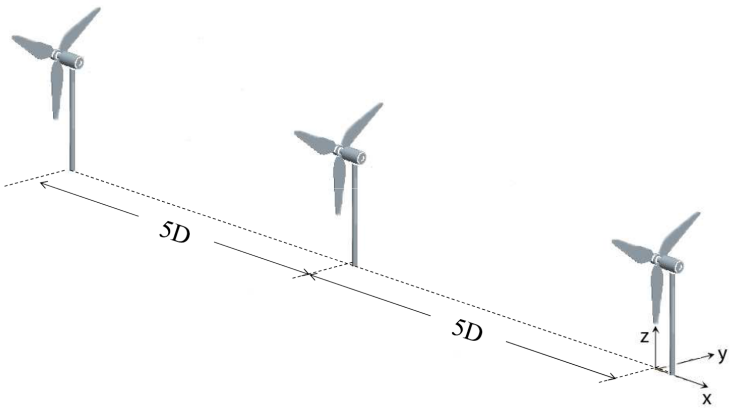

Figure 5. Three turbine setup aligned. Turbine 1 is the most upstream turbine, Turbine 2 is the middle turbine, and Turbine 3 is the most downstream turbine.

3.3.3. Measuring the Dynamic Response

In addition to PIV, voltage tests were used to characterize the input/output behavior of the three turbine setup with a goal of constructing a dynamic model of the input/output behavior of the three-turbine array. Several experiments were run to examine the dynamic response of Turbine 2 and Turbine 3 based on the inputs to Turbine 1. Square waves with varying frequencies were applied to the upstream turbine and the voltage response of the downstream turbines was recorded. Square waves were chosen as an input for convenience based on the function generator and power supplies available in the wind tunnel at the time of the experiments. These square waves varied in frequency from 0.02 Hz to 10 Hz with a 50% duty cycle. Specifically, the square wave varied from 0V (derated) to 1.25V (rated), i.e. the turbine was switching states at varying frequencies. By measuring the magnitude and phase of the power at Turbine 2 and Turbine 3, a dynamic model can be constructed that relates the input of Turbine 1 to the voltage output of Turbine 2 and Turbine 3 at different frequencies. The result is a model that can be used for design and analysis for coordinated turbine control in the wind tunnel.

Note that the frequencies in these experiments were chosen to inspect the ability of the model turbines to respond to a given input. At high frequencies, the downstream turbine response to an input at the upstream turbine is limited due to the internal electrical resistance, and primarily, the rotational inertia of the rotor. The frequencies chosen for the wind tunnel voltage experiments can be translated to relevant wind gust events for utility-scale turbines. The model turbine rotor speed was measured using a tachometer and was observed to be approximately 2400 RPM, or 40 Hz. Thus the voltage perturbation frequencies used in the experiments are between 0.0005 to 0.25 of the model rotor turbine speed. The Clipper turbine, in Figure 4, has a rotational frequency of around 0.2 Hz (one blade revolution completed in 5 s) while operating in the same region as the model turbine. The voltage perturbations used in the experiments thus scale to frequencies between 0.0001 Hz and 0.05 Hz (= 0.2*[0.0005 0.25]) for the Clipper turbine. Qualitatively, these time scales correspond to wind variations on the order of hours down to wind gusts, which can be on the order of tens of seconds [31].

4. RESULTS

4.1. Wake Characteristics - PIV

The experimental data gathered using PIV was first used to compute the mean velocity behind Turbine 1 to understand the overall effects of turbine control on the velocity behind the turbine. Figure 6 shows the mean wind speeds behind Turbine 1 in the rated and derated cases. This shows that when the upstream turbine is operating under higher thrust conditions (derated), the turbine blocks more of the flow, forcing the flow around the turbine, resulting in a larger velocity deficit directly behind the turbine than in the rated case. Figure 6 shows the growth of the turbine wake, as defined by the domain of its large scale meandering motions [19]. We note that the wake expansion in the y direction depends on the turbine operating condition. The edges of the wake are tracked in Figure 6c and 6d. The wake in the derated case expands from $0.5D$ directly behind the rotor to $0.82D$ at $3D$ downstream. In the rated case, the wake expands from $0.5D$ to $0.74D$. This means that the wake expands at an average of 6.1^o in the derated case and 4.5^o in the rated case. More details can be found in [19]. The flow is normalized by the freestream velocity at hub height.

This wake depiction, in Figure 6, varies from the Park model described in Section 2.2. Recall that the Park model assumed that the velocity in the wake was constant at a given cross section downstream. Figure 7 shows the spanwise

DOI: 10.1002/we
Prepared using weauth.cls

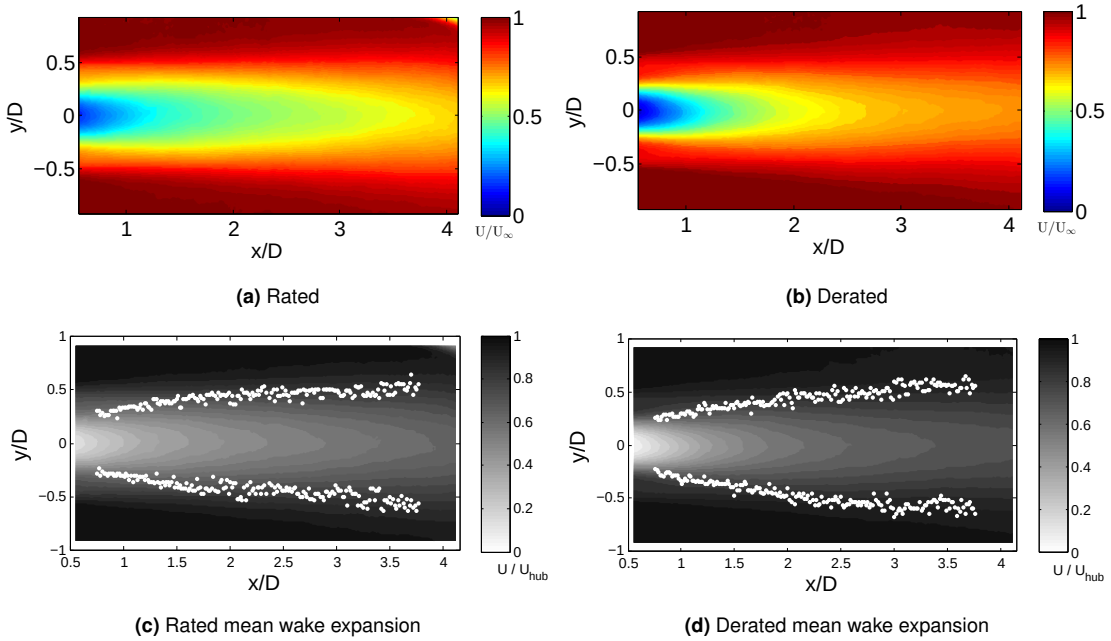

Figure 6. Mean streamwise velocity behind Turbine 1

velocity deficit at $1D$, $2D$, $3D$, and $4D$ downstream in the wake from PIV compared to the Park model assumption. This discrepancy can have a significant impact on control. Some studies have implemented modifications to the Park model by introducing different zones of the wake that provide a more accurate description of the wake [32]. An alternative approach may be to modify the Park model to incorporate a Gaussian velocity profile that evolves as a function of downstream distance [17].

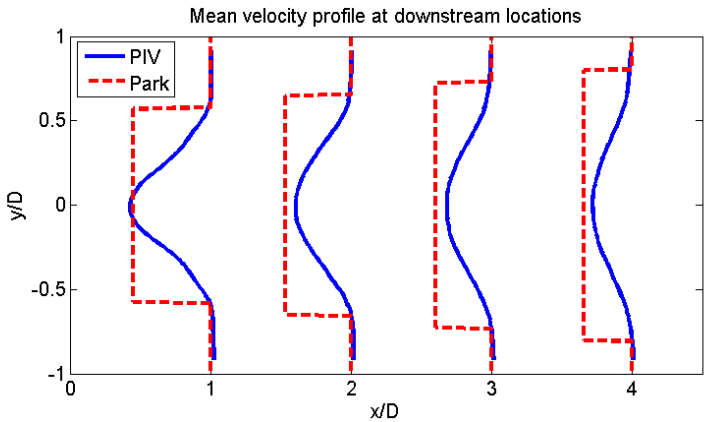

Figure 7. Time averaged spanwise velocity profile from PIV experiments compared to the spanwise profile obtained from the Park model

The mean velocity is also evaluated along the centerline, i.e. $y = 0$, to understand the effects of turbine control on the rate of wake recovery. Figure 8 shows the centerline mean velocity from Turbine 1 to Turbine 3. PIV data captured behind Turbine 1 as well as PIV data captured behind Turbine 2 are combined in Figure 8. The vertical black line indicates where Turbine 2 is located. These results are compared to the Park model. In the derated case, a k value of 0.15 best describes the centerline velocity, while a k value of 0.09 better describes the rated case. Recall (2), a single k, or wake expansion coefficient, is typically used to describe interactions in a wind farm across all operating conditions. The results in Figure 8 suggest that a single k value may not be able to capture the impact of different operating conditions nor is it able to accurately capture the wake recovery behind Turbine 2. This discrepancy has to do with the different turbulence levels and structures present in the wake.

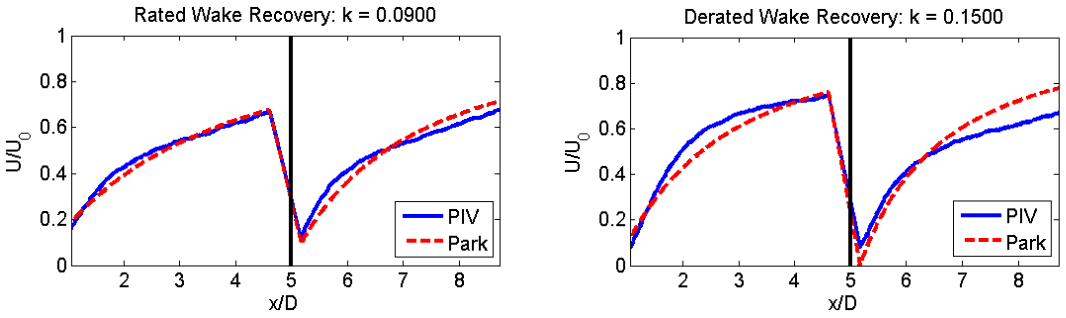

(a) Rated **(b)** Derated

Figure 8. Centerline velocity profile from Turbine 1 to Turbine 3. The vertical black line indicates where the second turbine is located

Figure 9 shows the turbulent kinetic energy (TKE) behind Turbine 1 in the rated and derated case. Specifically, when the rated case is compared to the derated case, there is noticeably more TKE in the case where the turbine is operating under higher loading conditions. This is due to the increase in the induction factor that was described in Section 2.2. This increase in turbulence leads to additional mixing in the wake, i.e. fluid outside the wake is entrained into the wake. This allows the wake to recover at a faster rate. As more fluid is entrained the wake expands, as seen in Figure 6c and Figure 6d. This suggests that, in the Park model, a single wake expansion coefficient, k, does not fully describe the various operating conditions in a wind farm. There have been some studies done to investigate this effect [33]. The Park model can be modified to incorporate the change in turbulence due to varying operating conditions. For example, the wake expansion coefficient, k, can be thought of as a function of the induction factor(s) of the upstream turbine(s) as is done in [28]. Specifically, as the induction factor of the upstream turbine(s) changes, the wake expansion coefficient would also change to accommodate the change in the turbulence level.

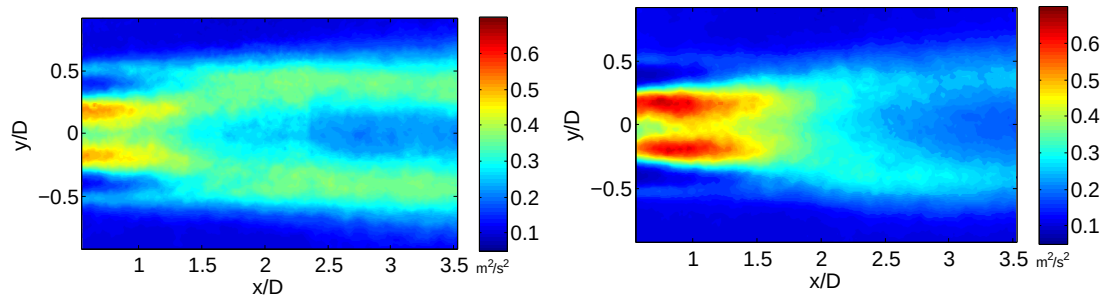

(a) Rated **(b)** Derated

Figure 9. Turbulent kinetic energy behind Turbine 1 under two operating conditions

4.2. Propagation Dynamics - Voltage Measurements

A complementary set of voltage input/output experiments was performed to understand the dynamics of the turbine array and to highlight the temporal limitations of the static Park model. Two different single-input-single-output models are considered in these experiments: the input voltage at Turbine 1 to the output voltage at Turbine 2 and the input voltage at Turbine 1 to the output voltage at Turbine 3. These models could be used to coordinate turbines in the wind tunnel.

Figure 10 displays a few selected voltage inputs to Turbine 1 (top row) and the voltage generated at Turbine 2 (middle row) and Turbine 3 (bottom row). The results shown are ensemble averages over the total number of periods contained in each 100 s experiment. Specifically, the results shown for 0.07 Hz, 0.2 Hz, and 2 Hz correspond to ensemble averages over 5, 20, and 200 periods, respectively. This is important to note because each plot corresponds to an ensemble average over a different number of periods. Notice in Figure 10 there is a 180^o lag between the voltage input at Turbine 1 and the voltage output at Turbine 2 at low frequencies. When the signal on the upstream turbine is in a rated state, this means that the turbine is operating at a higher efficiency, and is extracting more energy out of the wind and overall wake recovery is slower than in the derated case. When the upstream turbine is derated, the wake experiences a faster recovery rate due to increased mixing and TKE resulting in a higher wind speed at the downstream turbine. It is important to note that this was

observed under a neutral boundary layer with 10% turbulence intensity in the wind tunnel. It is possible that increasing the ambient turbulence and operating under different atmospheric stability conditions could decrease the significance of the changing TSR of the upstream turbine.

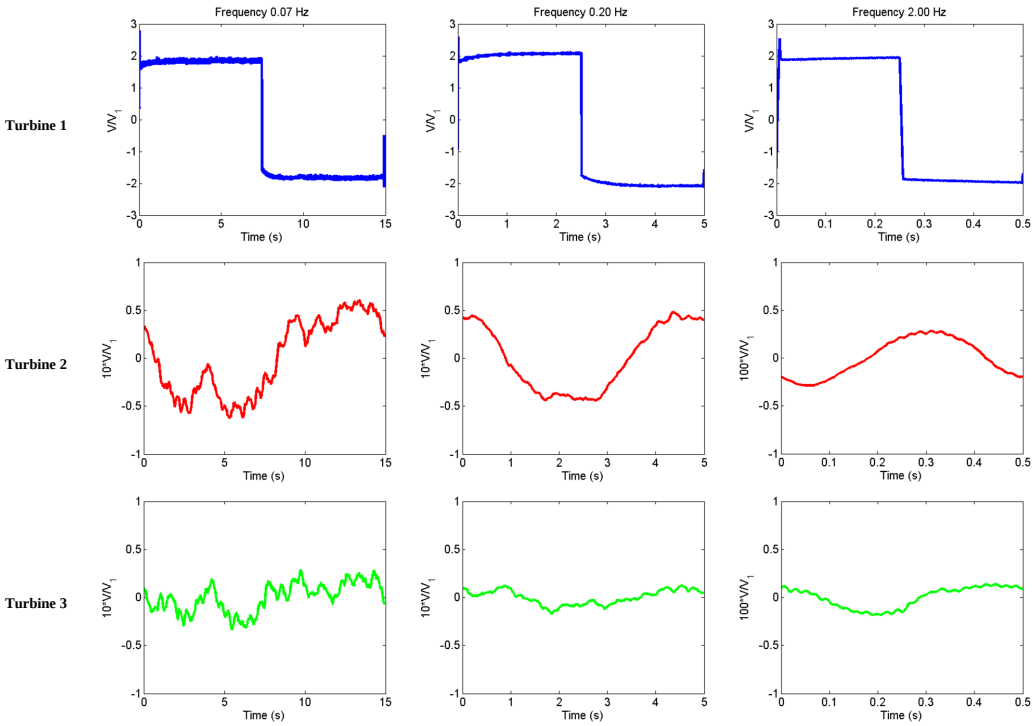

Figure 10. Voltage time series at 0.07 Hz, 0.2 Hz, and 2 Hz. Note that the signals for Turbine 2 and Turbine 3 have been scaled by a factor of 10 or 100 for visualization purposes.

As the frequency increases, the voltage production of Turbine 2 and Turbine 3 experiences a greater phase lag from the input at Turbine 1. For example, at 2 Hz (right column of Figure 10), the downstream turbine voltage responses experiences a greater phase lag than in the 0.07 Hz case. Turbine 2 and Turbine 3 do not respond instantaneously to the effects of Turbine 1. This is due to the time it takes for the effects of the input at Turbine 1 to propagate downstream and impact the performance of Turbine 2 and Turbine 3. At 2 Hz, the input at Turbine 1 is changing nearly as fast as it takes for the previous input to propagate downstream. This results in a phase lag greater than 360^o.

From the figures above, note the amplitudes of Turbine 2 and Turbine 3 are scaled by a factor of 10 for 0.07 Hz and 0.2 Hz and scaled by a factor of 100 for 2 Hz. This allows for better comparisons of the phase and magnitude between Turbines 1, 2, and 3. There is a significant decrease in amplitude between Turbine 2 and Turbine 3. Turbine 3 is located farther downstream from Turbine 1($10D$). The wake has more time to evolve from the control actions of Turbine 1. Lastly, the model turbines have a certain amount of rotational inertia that reduces the turbine response to fast frequencies. For example, a utility-scale turbine can respond to large gusts of wind, but due to its large rotational inertia, it cannot respond to the microscales of turbulence.

Frequency domain techniques were used to construct dynamic models from an upstream voltage input, u, to a downstream voltage output, y. For each experiment, the Fourier Transform of the domain data samples $\{u_k, y_k\}_{k=1}^{L}$ was computed. This data consists of complex numbers $\{\hat{U}(\omega_j), \hat{Y}(\omega_j)\}_{j=1}^{L}$ that depend on the frequency, ω_j. The power spectrums $(\hat{U}, \hat{Y})$ contain noise, e.g. due to 60 Hz electric interference. To eliminate the effects of this noise the ratio $\hat{G}(jf) = \hat{Y}(jf)/\hat{U}(jf)$ was computed only at the excitation frequency, f, of the square wave input. The magnitude and phase of this complex number, $\hat{G}$, computed for each experiment is shown as a function of frequency (green dots) in Figure 11. The magnitude is shown in units of decibels: $20\log_{10}|\hat{G}|$.

The dynamic Park model, described in Section 2.3, can be used construct a model that agrees with the frequency response of the experimental data and can provide additional physical insight into the system. In these experiments, the voltage input varied at Turbine 1. This voltage input can be thought of as the signal τ_{g1} in the block diagram in Figure 3. It is important to note that the DC motor on the scale model turbine (mentioned in Section 3) is not specifically modeled, i.e. the relation between input voltage on the scale turbine and generator torque on a utility-scale turbine is inexact. Similarly, the voltage input to Turbine 2 and Turbine 3, is held constant. These inputs correspond to τ_{g2} and τ_{g3}. Also, the wind speed input in the wind tunnel, U_∞, was held constant at 4.5 m/s. The measurements taken during these experiments include the voltage production, $P_{g,2}$ and $P_{g,3}$, at Turbine 2 and Turbine 3. This voltage production at Turbine 2 and Turbine 3 correspond to $P_{g,2}$ and $P_{g,3}$ in the block diagram, Figure 3. In these experiments, the connection between voltage output on the downstream turbines in roughly related to the power produced on a utility-scale turbine. The frequency plot shown in Figure 11a and 11b, shows the frequency response of the experiments from the input, τ_{g1} to the output, $P_{g,2}$ and the input, τ_{g1}, to the output $P_{g,3}$. This is compared to the frequency response from τ_{g1} to $P_{g,2}$ and τ_{g1} to $P_{g,3}$ using the dynamic Park model.

The parameters in the dynamic Park model (12) are estimated to fit the experimental data. Specifically, the physics of the dynamic Park model imply that the transfer function from Turbine 1 to Turbine 2 is parameterized by a DC (steady-state) gain, two real poles for the rotor dynamics, and a time delay for the convection of the wake. The DC gain of 0.0079 was fit as the mean of the low frequency magnitude data. The two real poles were selected as 2.5 rad/s to fit the roll-off in the magnitude data. Finally, a time delay of 0.22 s was selected to match the phase data. These parameters yielded the following gray-box model:

$$\hat{G}_{1\to 2} = \frac{-0.0497}{s^2 + 5s + 6.25} e^{-0.22s} \tag{14}$$

These parameters could be selected to optimally fit the experimental data, e.g. using `tfest` in the MATLAB® System Identification toolbox. However, this yielded second order systems with non-physical complex poles. Taylor's hypothesis of frozen turbulence can be used to provide an alternative estimate for the time delay. This hypothesis assumes that the turbulence is unchanged as it is advected downstream, i.e. transported by the wake from upstream to downstream. A consequence of this hypothesis is that the wake advection is only a function of the mean wind speed. For example, Turbine 1 and Turbine 2 are spaced $5D$, or 64 cm, apart with an inflow velocity of 4.5 m/s. As a result, the time delay should be approximately $\tau_d = 0.14$ s. This is a conservative estimate as the wake will be moving downstream at a reduced velocity, not the mean inflow velocity, due to the presence of the upstream turbine. Hence the larger delay in (14) is reasonable as it represent the effect of the slower velocity in the wake. A similar procedure was used to obtain the following fit from Turbine 1 to Turbine 3.

$$\hat{G}_{1\to 3} = \frac{-0.0439}{s^2 + 6s + 8.75} e^{-0.57s} \tag{15}$$

This second order model assumes that Turbine 2, which lies between Turbines 1 and 3, has negligible impact on the dynamics from Turbine 1 to 3 (although it may impact the steady state gain). This assumption will be investigated further in future work.

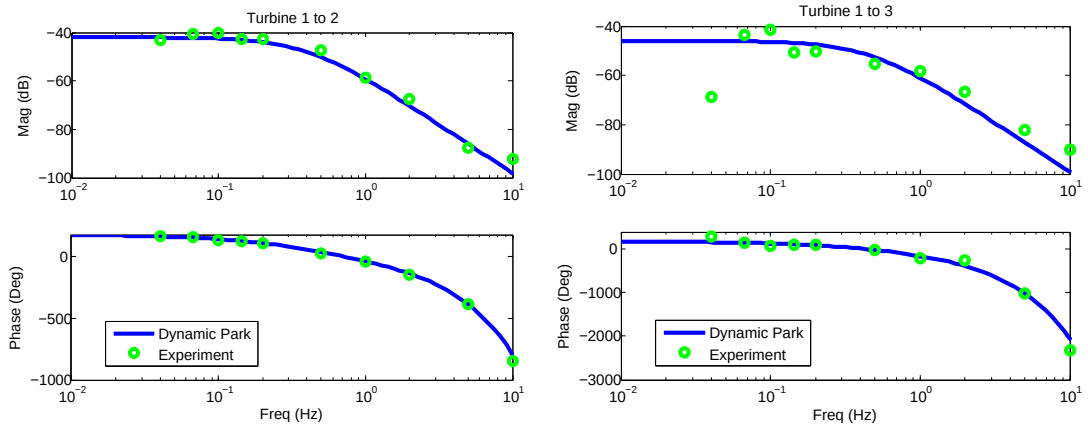

(a) Dynamic Response from Turbine 1 to Turbine 2

(b) Dynamics Response from Turbine 1 to Turbine 3

Figure 11. Input/output dynamics in the three turbine setup compared to the dynamic Park model

Wind Energ. 0000; **00**:1–15 © 0000 John Wiley & Sons, Ltd.
DOI: 10.1002/we
Prepared using weauth.cls

At low frequencies, Figure 11 shows that the model and experimental data are essentially static. However, as the frequency increases, the magnitude of the system rolls off, i.e. the downstream turbine does not have a significant response to inputs from Turbine 1 at frequencies greater than 0.5 Hz. The turbines are unable to respond to higher frequencies due to the rotational inertia of the turbine. In addition to the magnitude, the phase in Figure 11 contains the rotational dynamics of the turbine as well as information about the mean wake velocity. Specifically, the phase information from the experiments can be used to determine the approximate convection velocity in the wake. The amount of phase between the input and output response reflects how long the signal took to propagate through the flow field to the downstream turbine. Turbine 3 experiences a greater phase lag than Turbine 2 due to the distance from Turbine 1 and the time it takes to propagate the effects from Turbine 1 to Turbine 3. By analyzing the dynamic model in this way, we can get a sense of how the wake is evolving in time based on the input/output response of this three turbine array.

4.3. Example Model Application: Wind Farm Control

The dynamic Park model can be used to implement preliminary wind farm control strategies in the wind tunnel. A simple proportional-integral (PI) controller is implemented in simulation to demonstrate the potential applications of using the dynamic Park model for wind farm control in the wind tunnel. The PI controller had a proportional gain of -5 and an integral gain of -15. For simplicity turbulence is neglected. The dynamic Park model is used in the configuration seen in Figure 12a. The goal of this controller is to track the total power, or voltage in this case, produced by Turbine 2 and Turbine 3. This would be similar to a wind farm tracking a power command provided by the electric grid operators [34]. Due to limitations of the hardware, only the output voltages of Turbines 2 and 3 are able to be measured. The wind tunnel/scaled models currently do not allow for closed-loop control, e.g. they can only operate between a TSR of 3 and 4.5. These limitations are currently being addressed so that closed-loop experiments can be performed in the future.

Figure 12b shows the result of using a PI controller with the dynamic Park model. The top figure shows the simulated voltage input, τ_{g1} to Turbine 1 and the bottom figure shows the simulated closed-loop response, P_{TOT} of Turbine 2 and 3 to the input at Turbine 1. The green dotted-dashed line shows the baseline voltage output of Turbine 2 and Turbine 3 from the wind tunnel with no control from the experimental data. Although closed-loop control has not been used in the wind tunnel to date, we hope that closed-loop control will mitigate the issues of power loss, turbulence, and wake meandering in the wind turbine array in the wind tunnel.

Using a PI controller, the combined output voltage of Turbine 2 and 3 can follow a specific reference signal. In addition, Figure 12 shows that the turbines are able to respond quickly and accurately to a command. This type of control is significant for wind farms as they may be asked to follow specific energy dispatch signals as more wind is added to the electric grid [35],[34]. Power optimization of a wind farm is not specifically addressed in this paper and will be a future direction of this work.

5. CONCLUSIONS AND FUTURE WORK

An experimental investigation was conducted to analyze the effect of individual turbine control on wind farm dynamics and incorporate the findings to improve the existing static Park model. Model improvements included the incorporation of turbine dynamics that captured the input/output characteristics of a three-turbine array, which can be used for wind farm control in the wind tunnel. Wall parallel PIV was used to identify physical wake characteristics based on varying turbine operating conditions. Voltage tests were used to characterize the frequency response of the system.

Future work includes conducting more experiments with various turbine setups and developing control strategies around the dynamic models presented in this paper. Applying some modifications to the model turbines used in these experiments, we hope to perform wind farm control for simple turbine setups in the wind tunnel using the dynamic model developed in this paper.

6. ACKNOWLEDGEMENTS

This work was supported by the National Science Foundation under Grant No. NSF-CMMI-1254129 entitled CAREER: Probablistic Tools for High Reliability Monitoring and Control of Wind Farms. Any opinions, findings, and conclusions or recommendations expressed in this material are those of the authors and do not necessarily reflect the views of the NSF. In additions, the authors acknowledge support from the Institute on the Environment, University of Minnesota (Initiative for Renewable Energy and the Environment).

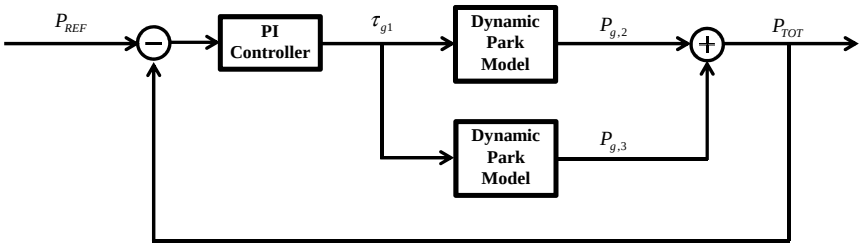

(a) PI control implemented using the dynamic Park model.

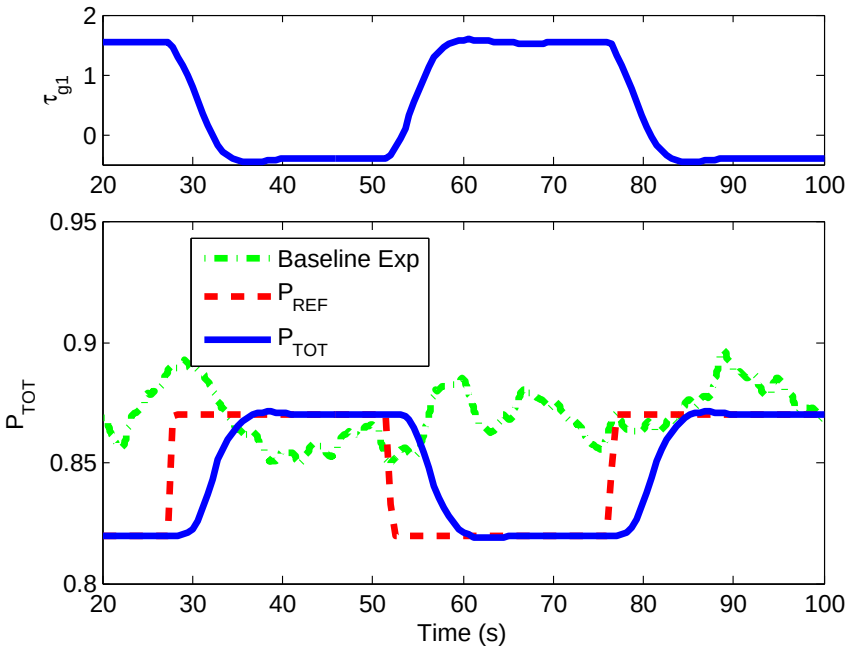

(b) Results of implementing a PI controller with the dynamic Park model. This is compared to the results from the wind tunnel with no control.

Figure 12. Simple control implementation using the dynamic Park model.

REFERENCES

1. Wiser R. Renewable portfolio standards in the United States - a status report with data through 2007. *LBNL-154E*, Lawrence Berkeley National Laboratory 2008.
2. Bitar E, Seiler P. Coordinated control of a wind turbine array for power maximization. *American Control Conference*, 2013; 2898–2904.
3. Gebraad P, Wingerden J. Maximum power-point tracking control for wind farms. *Wind Energy* 2014; .
4. Johnson KE, Thomas N. Wind farm control: Addressing the aerodynamic interaction among wind turbines. *American Control Conference*, 2009; 2104–2109.
5. Knudsen T, Bak T, Svenstrup M. Survey of wind farm control—power and fatigue optimization. *Wind Energy* 2014; .
6. Hong J, Toloui M, Chamorro LP, Guala M, Howard K, Riley S, Tucker J, Sotiropoulos F. Natural snowfall reveals large-scale flow structures in the wake of a 2.5-mw wind turbine. *Nature communications* 2014; **5**.
7. Medici D. Experimental studies of wind turbine wakes: power optimisation and meandering 2005; .
8. Knudsen T, Bak T. Data driven modelling of the dynamic wake between two wind turbines. *Sysid 2012 16th IFAC Symposium on System Identification Brussels*, vol. 16, 2012; 1677–1682.
9. Seem JE, Li Y. Systems and methods for optimizing power generation in a wind farm turbine array May 8 2012. US Patent App. 13/466,891.
10. Jensen NO. A note on wind generator interaction. *Technical Report Risø-M-2411*, Risø1983.

DOI: 10.1002/we
Prepared using weauth.cls

11. Ainslie JF. Calculating the flowfield in the wake of wind turbines. *Journal of Wind Engineering and Industrial Aerodynamics* 1988; **27**(1):213–224.
12. Hao Y, Lackner M, Keck RE, Lee S, Churchfield M, Moriarty P. Implementing the dynamic wake meandering model in the NWTC design codes. *AIAA*, 2013.
13. Koch F, Gresch M, Shewarega F, Erlich I, Bachmann U. Consideration of wind farm wake effect in power system dynamic simulation. *Power Tech, 2005 IEEE Russia*, IEEE, 2005; 1–7.
14. Choi J, Shan M. Advancement of jensen (park) wake model. *Proceedings of the European Wind Energy Conference and Exhibition*, 2013; 1–8.
15. González-Longatt F, Wall P, Terzija V. Wake effect in wind farm performance: Steady-state and dynamic behavior. *Renewable Energy* 2012; **39**(1):329–338.
16. Gebraad PM, Van Wingerden J. A control-oriented dynamic model for wakes in wind plants. *Journal of Physics: Conference Series*, vol. 524, IOP Publishing, 2014; 012 186.
17. Pope SB. *Turbulent flows*. Cambridge university press, 2000.
18. Sanderse B. Aerodynamics of wind turbine wakes. *Energy Research Center of the Netherlands (ECN), ECN-E–09-016, Petten, The Netherlands, Tech. Rep* 2009; .
19. Howard KB, Singh A, Guala M. On the statistics of wind turbine wake meandering: an experimental investigation Submitted to Physics of Fluids 2014; .
20. Chamorro LP, Porté-Agel F. Turbulent flow inside and above a wind farm: a wind-tunnel study. *Energies* 2011; **4**(11):1916–1936.
21. Okulov VL, Sorensen JN. Instability of the far wake behind a wind turbine. *Abs. 21th ICTAM-2004, Warsaw, Poland (http://ictam04. ippt. gov. pl/)* 2004; .
22. Kang S, Yang X, Sotiropoulos F. On the onset of wake meandering for an axial flow turbine in a turbulent open channel flow. *Journal of Fluid Mechanics* 2014; **744**:376–403.
23. Burton T, Jenkins N, Sharpe D, Bossanyi E. *Wind energy handbook*. John Wiley & Sons, 2011.
24. Johnson KE, Pao LY, Balas MJ, Fingersh LJ. Control of variable-speed wind turbines: standard and adaptive techniques for maximizing energy capture. *Control Systems, IEEE* 2006; **26**(3):70–81.
25. Sørensen T, Thøgersen ML, Nielsen P, Jernesvej N. Adapting and calibration of existing wake models to meet the conditions inside offshore wind farms. *EMD International A/S. Aalborg* 2008; .
26. Katic I, Højstrup J, Jensen N. A simple model for cluster efficiency. *EWEC* 1986; :407–410.
27. Marden JR, Ruben S, Pao L. A model-free approach to wind farm control using game theoretic methods. *IEEE Transactions on Control Systems Technology* 2013; :1207–1214.
28. Annoni J, Gebraad PM, Scholbrock AK, Fleming PA, van Wingerden JW. Analysis of axial-induction-based wind plant control using an engineering and a high-order wind plant model. *Wind Energy* 2015; .
29. Singh A, Howard KB, Guala M. On the homogenization of turbulent flow structures in the wake of a model wind turbine. *Physics of Fluids (1994-present)* 2014; **26**(2):025 103.
30. Howard K, Hu J, Chamorro L, Guala M. Characterizing the response of a wind turbine model under complex inflow conditions. *Wind Energy* 2014; .
31. Stull RB. *An introduction to boundary layer meteorology*, vol. 13. Springer, 1988.
32. Gebraad P, Teeuwisse F, Wingerden J, Fleming P, Ruben S, Marden J, Pao L. Wind plant power optimization through yaw control using a parametric model for wake effects—a cfd simulation study. *Wind Energy* 2014; .
33. Andersen SJ, Ivanell S, Mikkelsen R, *et al.*. Comparison of engineering wake models with CFD simulations. *Journal of Physics: Conference Series*, vol. 524, IOP Publishing, 2014; 012 161.
34. Wang S, Seiler P. Gain scheduled active power control for wind turbines. *AIAA Atmospheric Flight Mechanics Conference*, 2014.
35. Aho J, Buckspan A, Laks J, Fleming P, Jeong Y, Dunne F, Churchfield M, Pao L, Johnson K. A tutorial of wind turbine control for supporting grid frequency through active power control. *American Control Conference (ACC), 2012*, IEEE, 2012; 3120–3131.